Low-Temperature Matrix Isolation Studies of $BCl(N_3)_2$: Infrared Spectra and Photolysis Processes

Michael J. Travers, Erika L. Eldenburg, and Julanna V. Gilbert*

Department of Chemistry and Biochemistry, University of Denver, Denver, Colorado 80208

Received: June 10, 1999

$BCl(N_3)_2$ was isolated in a low-temperature argon matrix and its FTIR spectrum measured. The splitting due to the natural abundances of ^{10}B and ^{11}B and ab initio calculations of the ground-state frequencies support the identification of the IR spectrum. The observed frequencies for the ^{10}B species are 2165, 2161, 1371, 1354, and 1029 cm^{-1}. Upon UV photolysis, the $BCl(N_3)_2$ peaks decreased, and new peaks appeared at 1677 and 1724 cm^{-1} with a 4:1 intensity ratio, indicating a single B atom containing molecule. Based on ab initio calculations, the known photolysis mechanisms for similar compounds and the isotopic splitting, these peaks are assigned as the ring-breathing mode in $ClBN_2$, a compound in which the B and the two N atoms form a three-membered ring.

Introduction

Studies of group III azide systems are of fundamental and practical interest to chemists. Some of these molecules have been shown to decompose photolytically and thermally to generate group III−V films under room-temperature conditions.[1,2] Understanding the mechanism by which these processes take place adds to the general body of information regarding azide chemistry and to the details of film formation in these systems. To probe the mechanism by which this decomposition takes place, low-temperature matrix isolation studies have been carried out in our laboratory.[3,4] The first series of compounds studied are the boron-azide containing molecules generated via the gas-phase reaction between HN_3 with BCl_3. Three compounds can be formed, $BCl_2(N_3)$, $BCl(N_3)_2$, or $B(N_3)_3$, by adjusting the HN_3/BCl_3 ratio to 1:1, 2:1 and 3:1, respectively. The reaction of HN_3 and BCl_3 eliminates HCl and is assumed to proceed in a stepwise mechanism as shown in Table 1.[1]

The 3:1 product, $B(N_3)_3$, was first identified in gas-phase studies. In this work, BN film formation was observed via photolytic or thermal decomposition of the $B(N_3)_3$.[1] To gain information regarding the mechanism by which the photolytic decomposition takes place, $B(N_3)_3$ was deposited in low-temperature argon matrices and photolyzed. The photolytic intermediate, NNBN, was identified on the basis of its infrared spectrum and ab initio calculations.[3,5] The formation of BN films from linear NNBN is being examined computationally, and it appears likely that the mechanism consists of self-assembly of NNBN molecules.[6] The 1:1 product, BCl_2N_3, has also been isolated and photolyzed in low-temperature argon matrices. The linear compound ClBNCl, again identified on the basis of its infrared spectrum and ab initio calculations, was generated from the photolysis of BCl_2N_3.[4] For both the 3:1 compound, $B(N_3)_3$, and the 1:1 compound, $BCl_2(N_3)$, it is assumed that photolysis initially generates the trigonal fragments BN_3 and BCl_2N, respectively, followed by rearrangement to the linear forms, NNBN and ClBNCl.

Because of the stepwise nature of the $HN_3 + BCl_3$ reaction, an excess of HN_3 or BCl_3 was used in order to selectively generate the 3:1 or 1:1 product, respectively. In some of the 1:1 matrices generated, however, there were peaks in the BN stretching region of the IR spectra (1300−1400 cm^{-1}) that displayed photolysis rates that differed from the rates observed for peaks assigned to the 1:1 compound. It is now known that these anomalous features were due to the 2:1 compound, and that they appeared whenever there was not a sufficient excess of BCl_3 reagent. To generate matrices in which the 2:1 product dominated the others required extremely careful 2:1 stoichiometric control of the HN_3/BCl_3 ratio at all times during the deposition. This paper presents the IR spectrum of $BCl(N_3)_2$ in a low-temperature argon matrix and of the intermediates generated during UV photolysis. Ab initio calculations are also presented to support the IR assignments.

TABLE 1: Proposed Mechanisms for the Synthesis of $BCl_2(N_3)$, $BCl(N_3)_2$, and $B(N_3)_3$, Generated from 1:1, 2:1, and 3:1 HN_3/BCl_3 Stoichiometric Ratio

HN_3/BCl_3 ratio	proposed mechanism	net reaction
1:1	$HN_{3(g)} + BCl_{3(g)} \rightarrow BCl_2(N_3)_{(g)}$	$HN_{3(g)} + BCl_{3(g)} \rightarrow BCl_2(N_3)_{(g)}$
2:1	$HN_{3(g)} + BCl_{3(g)} \rightarrow BCl_2(N_3)_{(g)}$	$HN_{3(g)} + BCl_{3(g)} \rightarrow BCl(N_3)_{2(g)}$
	$HN_{3(g)} + BCl_2(N_3)_{(g)} \rightarrow BCl(N_3)_{2(g)}$	
3:1	$HN_{3(g)} + BCl_{3(g)} \rightarrow BCl_2(N_3)_{(g)}$	$3HN_{3(g)} + BCl_{3(g)} \rightarrow B(N_3)_{3(g)}$
	$HN_{3(g)} + BCl_2(N_3)_{(g)} \rightarrow BCl(N_3)_{2(g)}$	
	$HN_{3(g)} + BCl(N_3)_{2(g)} \rightarrow B(N_3)_{3(g)}$	

Experimental Section

$BCl(N_3)_2$ was prepared at room temperature in the gas phase by combining HN_3 and BCl_3. HN_3 was synthesized via the NaN_3 plus excess stearic acid reaction,[7] and the BCl_3 was obtained from Matheson. HN_3 is an explosive and toxic substance and must be handled with care. Both reagents were diluted with argon to 1% in five-liter glass Pyrex bulbs. The apparatus used for this work, consisting of a gas handling manifold coupled to a RMC model 22 cryostat, has been previously described in detail.[3]

Calculations were performed with *Gaussian 94* on a Silicon Graphics Octane work station.[8]

10.1021/jp991898l CCC: $18.00
Published on Web 11/11/1999

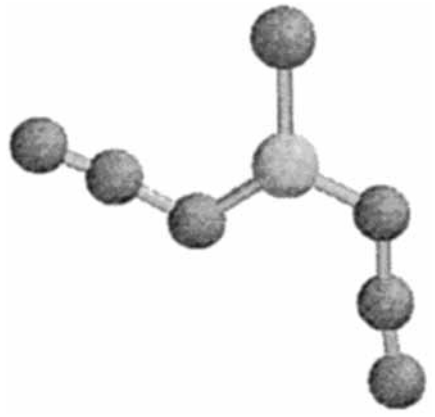

Figure 1. Calculated structure of $BCl(N_3)_2$.

TABLE 2: Optimized Ground State Geometry for $BCl(N_3)_2$[a]

parameter	MP2/6-31G(d) (bond lengths in Å, angles in deg)
B−N^a	1.4312
$N^a{}_\alpha$−N_β	1.2420
N^aN_β−N_γ	1.1670
B−N^b	1.4410
$N^b{}_\alpha$−N_β	1.2409
N^bN_β−N_γ	1.1662
B−Cl	1.7485
B−$N^a{}_\alpha$−N_β angle	120.2
$N^a{}_\alpha$−N_β−N_γ angle	172.5
B−$N^b{}_\alpha$−N_β angle	121.7
$N^b{}_\alpha$−N_β−N_γ angle	173.2
N^a-B−N^bangle	118.7
N^a-B−Cl angle	118.0
N^b-B−Cl angle	123.3

[a] The molecule is predicted to be nearly planar.

Results and Discussion

Ab Initio Calculations. With the 2:1 HN_3/BCl_3 reagent ratios used in this experiment, the predicted product was $BCl(N_3)_2$, a molecule that has not been reported previously. As a part of the investigation of the 3:1 and 1:1 adducts, $B(N_3)_3$ and BCl_2N_3, geometry optimization and ground-state frequencies for the ^{11}B and the ^{10}B isotopomers were computed with *Gaussian 94* at the MP2 level of theory utilizing the 6-31G(d) basis set.[3,4,8] These calculations gave ground-state frequencies that were within 6% of those observed and calculated boron isotope shifts that were in excellent agreement with the observed shifts for these compounds in low-temperature argon matrices. Hence, analogous calculations were carried out for the 2:1 adduct. The optimized structure obtained is shown in Figure 1, with the bond lengths and bond angles tabulated in Table 2, and the ground-state frequencies included in Table 3.

Infrared Spectrum of $BCl(N_3)_2$. From the infrared spectra of the matrices prepared for study of the 2:1 compound it was clear that the 3:1 and/or the 1:1 adduct were also present. The spectra, however, consistently displayed features that could not be assigned to either of these previously characterized molecules. A typical example of such a spectrum is presented in Figure 2, with prominent new peaks appearing at 2161 and 1371 cm^{-1} and weak features between 950 and 1200 cm^{-1}. This spectrum is similar to the IR spectra of $B(N_3)_3$ and $BCl_2(N_3)$ in argon matrices, with the strong features in the N_3 asymmetric and BN stretching regions and the weak features in the N_3 symmetric and the BCl stretching regions.

The N_3 Asymmetric Stretching Region. Examination of the N_3 asymmetric stretching region of a 2:1 sample, yields, in addition to the major peak at 2161 cm^{-1}, a shoulder at 2158 cm^{-1} and peaks at 2170 and 2165 cm^{-1}. The growth behavior observed as the matrix was deposited (Figure 3A) shows that the 2170 cm^{-1} peak grows in rapidly at the beginning of the deposition, and then slows down relative to the 2161 cm^{-1} feature. The 2165 cm^{-1} peak appears to grow in at the same rate as the 2161 cm^{-1} feature throughout the deposition, while the shoulder at 2158 cm^{-1} only appears toward the end of the deposition.

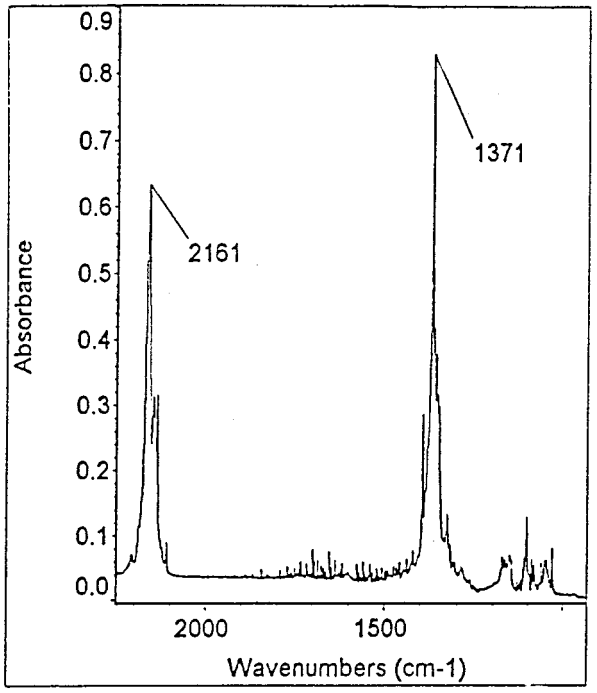

Figure 2. IR spectrum of a low-temperature argon matrix prepared with a HN_3/BCl_3 ratio of 2:1.

From a comparison of this region to the same spectral regions of a 3:1 matrix (Figure 4A) and of a 1:1 matrix (Figure 5A), the 2158 cm^{-1} and 2170 cm^{-1} features are assigned to $B(N_3)_3$ and BCl_2N_3, respectively. The 2161 and 2165 cm^{-1} peaks indicate the presence of a new species in the 2:1 sample. The $BCl(N_3)_2$ calculations predict two N_3 asymmetric stretching modes, one in which the center N atoms of the two azide groups are moving in concert (labeled a-ss in Table 3) and one in which they are moving in opposing directions (labeled a-as in Table 3). The observed peaks at 2165 and 2161 cm^{-1} are assigned to these modes.

The growth behavior implies that at the beginning of the deposition the HN_3/BCl_3 ratio was lower and at the end of the deposition was higher than the optimum ratio required for the production of a 2:1 adduct.

The BN Stretching Region. Figure 3B shows the BN stretching region of the IR spectrum of the 2:1 sample during deposition. Peaks appear at 1393, 1371, 1358, 1354, and 1350 cm^{-1}. From a comparison of the BN region of the 2:1 sample matrix spectrum to the same regions of $B(N_3)_3$ and BCl_2N_3 matrix spectra (Figures 4B and 5B), the 1358 and 1350 cm^{-1} peaks are assigned to $B(N_3)_3$ and BCl_2N_3, respectively. The 1354 cm^{-1} feature does not appear either in the $B(N_3)_3$ or BCl_2N_3 spectrum and is assigned to a new species in the 2:1 sample. The remaining two peaks at 1371 and 1393 cm^{-1} are assumed to be due to the boron isotopomers of the new species because of their 4:1 intensity ratio. Determining the species responsible for these two peaks was somewhat complicated by the fact that

TABLE 3: Calculated and Observed Infrared Frequencies for $BCl(N_3)_2$[a]

	υ_{13}	υ_{14}	υ_{15} (BN ss)	υ_{16} (BN as)	υ_{17} (N_3 a-as)	υ_{18} (N_3 a-ss)
			Argon Matrix			
$^{11}BCl(N_3)_2$	1029(10)[b]		1354[c]	1371(100)	2161(76)	2165[d]
$^{10}BCl(N_3)_2$	1060[b]			1393		
difference	31			22		
			Calculated Frequencies [MP2/6-31G(d)]			
$^{11}BCl(N_3)_2$	1097(350)	1127(149)	1395(219)	1449(880)	2178(578)	2193(499)
$^{10}BCl(N_3)_2$	1130	1148	1405	1472	2178	2193
difference	33	21	10	23		

[a] The notation is defined as follows: ss − symmetric stretch, as − asymmetric stretch, a-as − asymmetric−asymmetric stretch and a-ss − asymmetric-symmetric stretch. The numbers in parentheses are relative intensities for the experimental data and intensities in km/mol for the calculated data. [b] Peaks are assigned as shown based on the frequency separation between the ^{10}B and ^{11}B isotopomers. [c] This feature appears between peaks assigned as BN stretches in $B(N_3)_3$ and BCl_2N_3 in matrices containing 1:1, 2:1, and 3:1 compounds. [d] The relative intensity cannot be obtained for this feature since it is not sufficiently resolved. It is, however, less intense than the 2161 cm^{-1} peak.

they appear in both the 2:1 sample spectrum and the $B(N_3)_3$ spectrum. In the $B(N_3)_3$ spectrum, the three peaks at 1358, 1365, and 1371 cm^{-1} were assigned to BN stretching modes associated with different matrix sites with the three weak features to the blue assigned as the BN modes in the corresponding ^{10}B isotopomers. Possible explanations as to why the 1371 cm^{-1} feature appears in both the $B(N_3)_3$ spectrum and in the spectrum of the 2:1 sample are that (1) the features are due to the same molecule present in both samples or (2) there is a near-coincident frequency in the 3:1 adduct and the new species present in the 2:1 sample. Even though the presence of $B(N_3)_3$ in the 2:1 sample is evident, information extracted from the examination of IR spectra of many prepared matrices strongly supports the second explanation. In the $B(N_3)_3$ work, it was reported that the relative intensities of the three BN features (see Figure 4B) varied from matrix to matrix. It is now clear, however, that this variation can be correlated with the HN_3/BCl_3 ratio. Whenever the HN_3/BCl_3 was 10:1 or larger, the 1371 cm^{-1} peak was less intense than the 1358 cm^{-1} peak and the BN region was as shown in Figure 4B. Under these conditions, it is very unlikely that significant amounts of the 2:1 adduct could be generated. The only circumstances for which the 1371 cm^{-1} peak was more intense than the 1358 cm^{-1} peak was when the HN_3/BCl_3 ratio was less than 10:1 (but still 3:1 or larger). Under these conditions, detectable amounts of the 2:1 adduct could be generated and deposited in the matrix.

The deposition growth behavior (Figure 3B) of this region is consistent with the assignment of the 1371, 1393, and 1354 cm^{-1} features to a new species. The peaks at 1371 and 1350 cm^{-1} appear first, with the 1371 cm^{-1} peak rapidly dominating the 1350 cm^{-1} feature as the deposition proceeds. The peak at 1358 cm^{-1} emerges later during the deposition. This is in agreement with what was observed in the N_3 region if the 1371 cm^{-1} peak is assigned to a new species. Initially, the ratio is lower than required for optimum production of the 2:1 species and the 1:1 adduct is preferentially generated; at the end the ratio is higher than required and the 3:1 adduct is preferentially generated.

Two BN stretching frequencies, one at 1449 cm^{-1} (the asymmetric stretch) and one at 1395 cm^{-1} (the symmetric stretch), are calculated. The two features in the BN region associated with the 2:1 sample at 1371 and 1354 cm^{-1} are assigned to be these BN modes. Isotope shifts, which are routinely used as a test of calculated structures, are included in Table 3. The agreement between the observed and calculated shifts for the BN asymmetric stretch is excellent, supporting the assignment of the 1371 cm^{-1} feature to the asymmetric BN stretch in $BCl(N_3)_2$ and the 1393 cm^{-1} peak to the same mode in the ^{10}B isotopomer. The ^{10}BN symmetric stretch is calculated to be 10 cm^{-1} to the blue of the ^{11}BN symmetric stretch but cannot be observed because of the congestion in the spectrum.

The calculations predict that the BN asymmetric stretch is more intense than the N_3 asymmetric stretches, and this is consistent with what is observed. These features are calculated to have about the same intensity for the 3:1 and 1:1 compounds, again, consistent with what is observed.

The N_3 Symmetric and BCl Stretching Regions. Figure 3C shows the N_3 and BCl spectrum of the 2:1 sample as it was deposited. Figures 4C and 5C compare this region to the same regions in $B(N_3)_3$ and BCl_2N_3, respectively. Although the features in this region are weak in the spectrum of the 2:1 sample, the two distinct features at 1029 and 1060 cm^{-1} appear consistently in the 2:1 samples and do not appear in the spectra of either the 3:1 or 1:1 adducts. It is clear that these two features are due to a new species formed when the HN_3/BCl_3 ratio is 2:1.

Because of the agreement between the calculated and observed boron isotope shift for the BCl stretch (Table 3), the 1029 cm^{-1} peak is assigned to the BCl stretch. The intensity ratio of the 1029 cm^{-1} to the 1060 cm^{-1} peaks is somewhat smaller than 4:1; however, this is likely due to the unreliability of the baseline correction for these weak features. There is a relatively broad feature between the 1029 and 1060 cm^{-1} peaks that may be associated with the N_3 symmetric stretches (ν_{14}) in $BCl(N_3)_2$; however, there is no clear evidence of a feature that could be assigned to the ^{10}B isotopomer 21 cm^{-1} to the blue (predicted by the calculations), so no assignment for this feature is made.

Values for the relative intensities of the observed spectrum and for the calculated intensities are included in parentheses following the observed and calculated frequencies in Table 3. A major discrepancy between these occurs for υ_{13}, the BCl stretching mode. The poor agreement for the observed and calculated intensities relative to the intensity for υ_{16}, the mode that displays the highest intensity, suggests that the calculated charge distribution is incorrect. This mode was, however, assigned on the basis of the very good agreement between the observed and calculated boron isotope splitting. Such agreement is indicative of the fact that the calculated geometry is very close to the true geometry. So that the IR spectra of the 1:1, 2:1, and 3:1 adducts can be compared, the observed spectral features are listed in Table 4.

Photolysis of $BCl(N_3)_2$. If the new features observed at 2161, 1393, 1371, 1060, and 1029 cm^{-1} in the IR spectra of matrices prepared with 2:1 HN_3/BCl_3 reagent ratios are due to the 2:1 adduct, $BCl(N_3)_2$, then these features must display the same photolysis behavior. Upon photolysis with the loosely focused output of a D_2 lamp, all of these peaks (as well as the BCl_2N_3 and the $B(N_3)_3$ peaks) were observed to decrease. Infrared spectra as a function of photolysis time are shown in Figure 6, for a matrix that contained both 2:1 and 3:1 compounds, and in

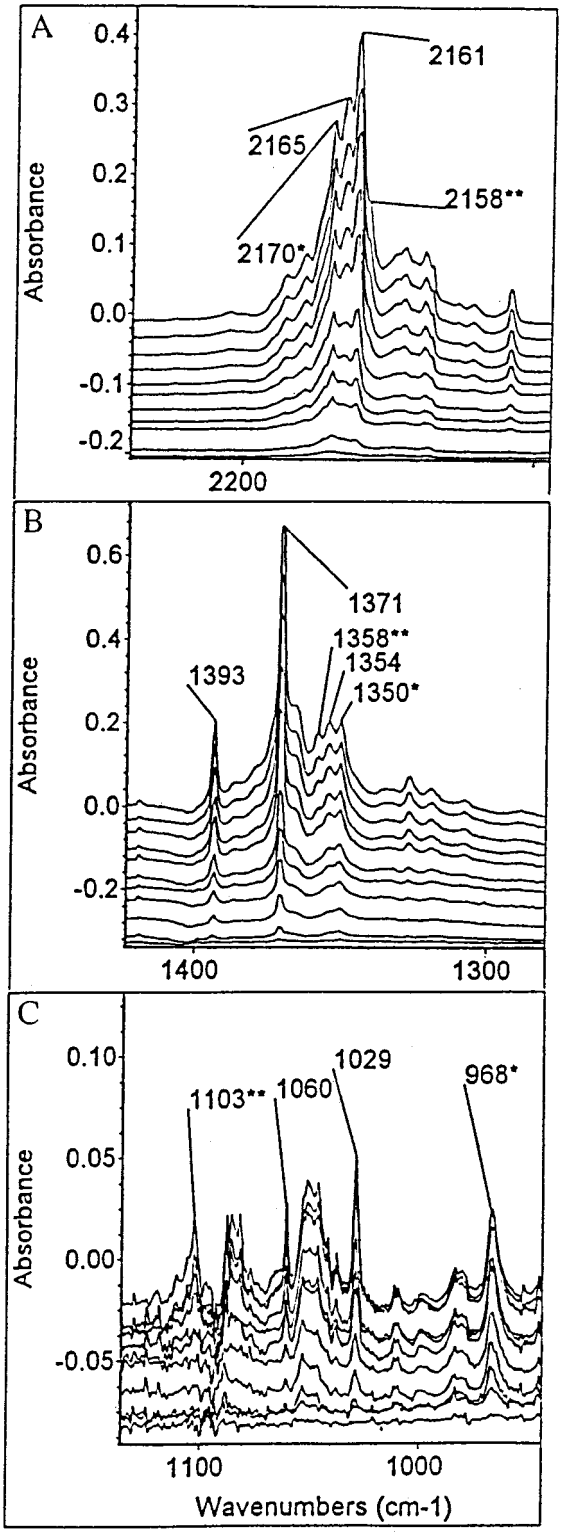

Figure 3. IR spectra taken during deposition of an argon matrix with a 2:1 HN_3/BCl_3 ratio. (A) N_3 asymmetric stretching region, (B) BN stretching region, and (C) N_3 symmetric and BCl stretching regions. There were apparently small variations in the stoichiometric ratio during the deposition, since at the beginning of the deposition the 1:1 product (BCl_2N_3) is deposited (* peaks), but, as the deposition proceeds, the 2:1 product ($BCl(N_3)_2$) clearly appears and overtakes the 1:1 product. Small amounts of the 3:1 product ($B(N_3)_3$) were also deposited (** peaks).

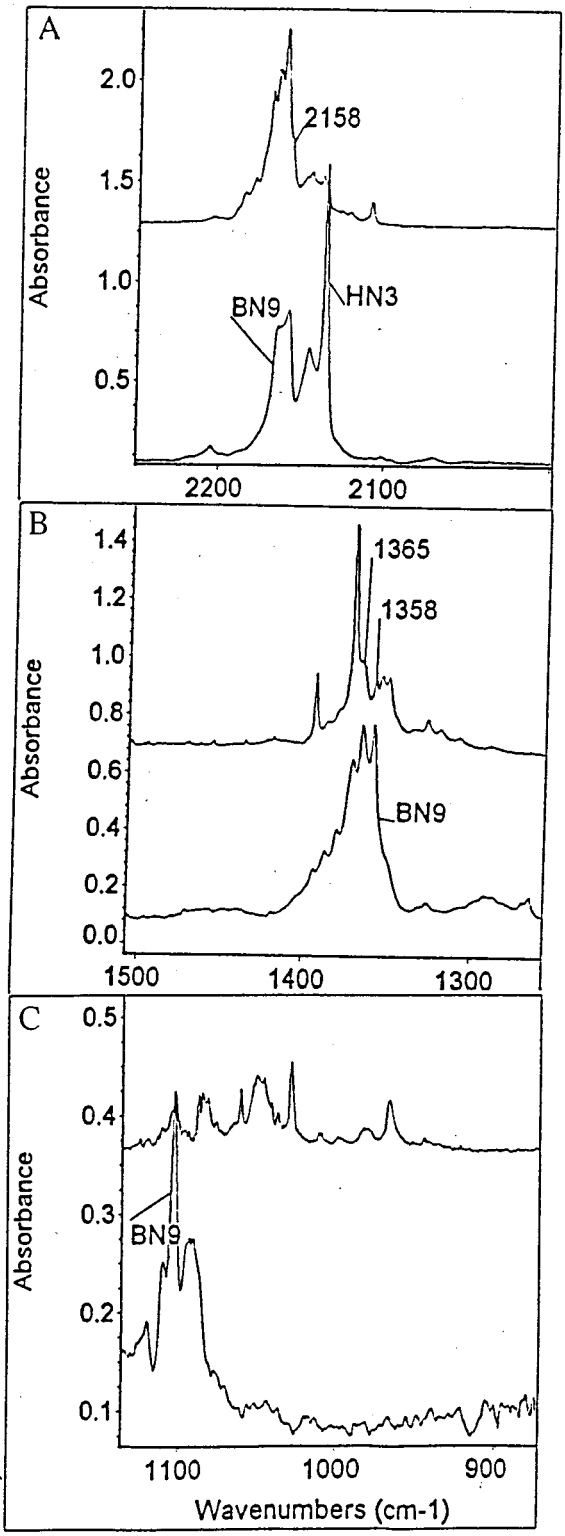

Figure 4. Comparison of the IR spectra for the 2:1 product and the 3:1 product ($B(N_3)_3$). (A) N_3 asymmetric stretching region, (B) BN stretching region, and (C) N_3 symmetric and BCl stretching region.

Figure 7, for a matrix that contained both 2:1 and 1:1 compounds. Plots of normalized intensities of peaks from Figures 6 and 7 as a function of photolysis time are shown in Figure 8. The fact that the 2:1 and 3:1 compounds display the same photolysis rate (Figure 8A) is one reason that, in our first studies of $B(N_3)_3$, it was assumed that both the 1350 and the 1371 cm^{-1} peaks were due only to $B(N_3)_3$. Figure 8B shows that the 2:1 compound, on the other hand, has a faster photolysis rate than that of the 1:1 compound. The 2:1 decay rates differ in Figures 8A and 8B because these data were collected for two different matrices on two different days for which the

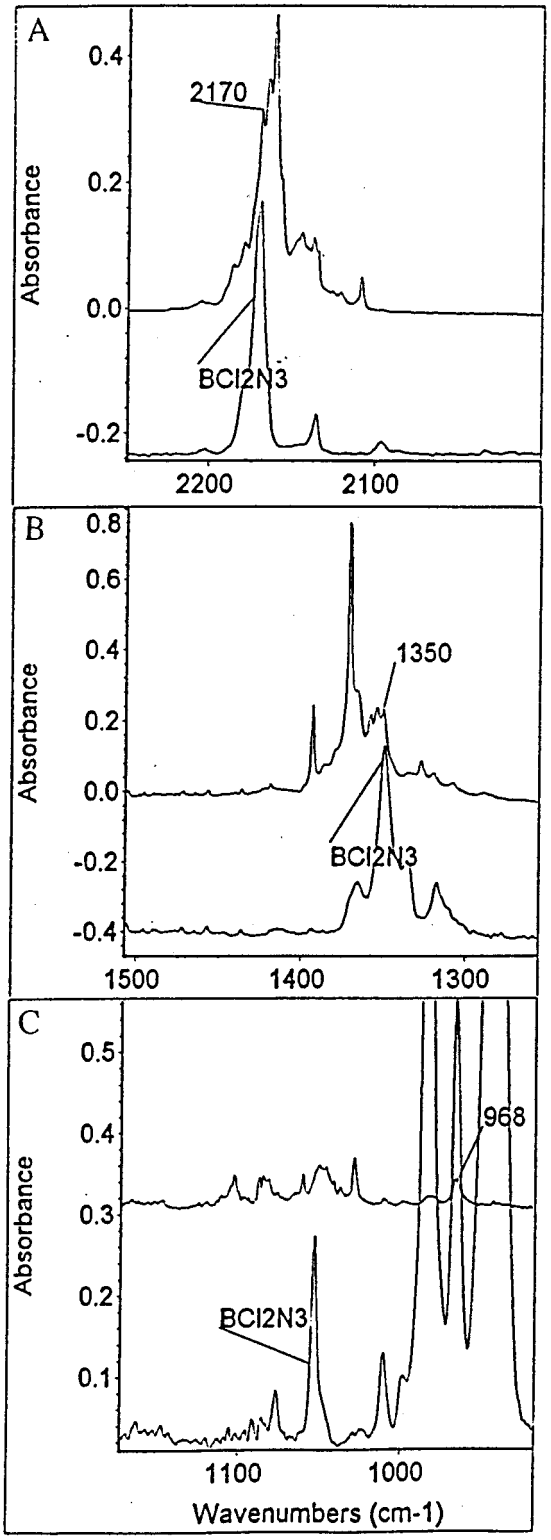

Figure 5. Comparison of the IR spectrum for the 2:1 product and the 1:1 product ($BCl_2(N_3)$). (A) N_3 asymmetric stretching region, (B) BN stretching region, and (C) N_3 symmetric and BCl stretching region.

photolysis conditions were not identical (for example, different UV lamp intensities, different light scattering characteristics of the matrix, etc.).

As the photolysis proceeds, other changes are observed in the spectrum as shown in Figure 9. In matrices that contain $BCl(N_3)_2$ and $B(N_3)_3$, features at 2100, 1861, 1803, 1724, and 1677 cm^{-1} grow in steadily and a peak at 2050 cm^{-1} grows in and then decays during the photolysis (Figure 9A). In matrices

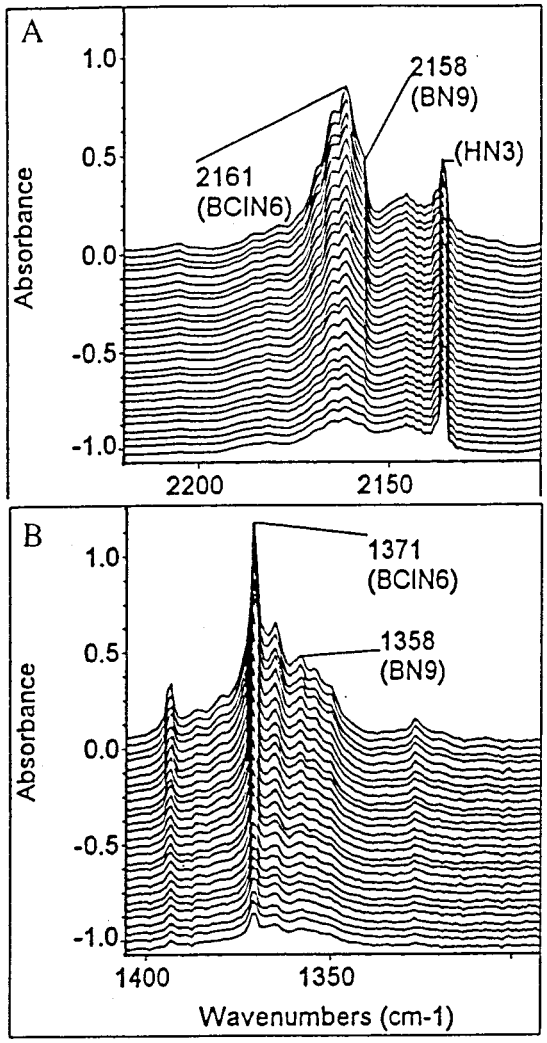

Figure 6. Changes occurring in the IR spectrum during photolysis of an argon matrix containing $B(N_3)_3$ and $BCl(N_3)_2$. (A) N_3 asymmetric and (B) BN stretching regions. The top spectrum was taken just before the photolysis began and the bottom spectrum was taken after 2 h of photolysis.

that contain $BCl(N_3)_2$ and BCl_2N_3, features at 2087, 2034, 1724, and 1677 cm^{-1} grow steadily (Figure 9B). Again, a peak at 2050 cm^{-1} grows in and then decays as the photolysis proceeds. Some of these peaks are readily assigned based on the previous photolysis studies of $B(N_3)_3$ and BCl_2N_3. The 2100, 1861, and 1803 cm^{-1} peaks are due to the generation of NNBN from the photolysis of $B(N_3)_3$, and the 2087 and 2034 cm^{-1} peaks indicate the production of ClBNCl from the photolysis of BCl_2N_3. The 1724 and 1677 cm^{-1} features have not been observed in 3:1 or 1:1 matrices, and their intensity ratio of 1:4 strongly suggests that a species containing a single B atom is responsible. The fact that the 2050 cm^{-1} displays a different photolytic behavior than does the 1677/1724 cm^{-1} pair indicates the presence of a second, photolytically unstable product.

To identify the product formed from the photolysis of $BCl(N_3)_2$, it was assumed that the photolytic mechanism was analogous to that observed in the 3:1 and 1:1 cases. In those samples, the linear compounds NNBN and ClBNCl, were observed, stable molecules that are isoelectronic with isocyanogen and dichloroacetylene. In both cases, it was assumed that the photolysis produced an unstable, trigonal intermediate (either BN_3 or $BNCl_2$) that underwent rearrangement to the final form observed in the matrix environment. For the 2:1 system,

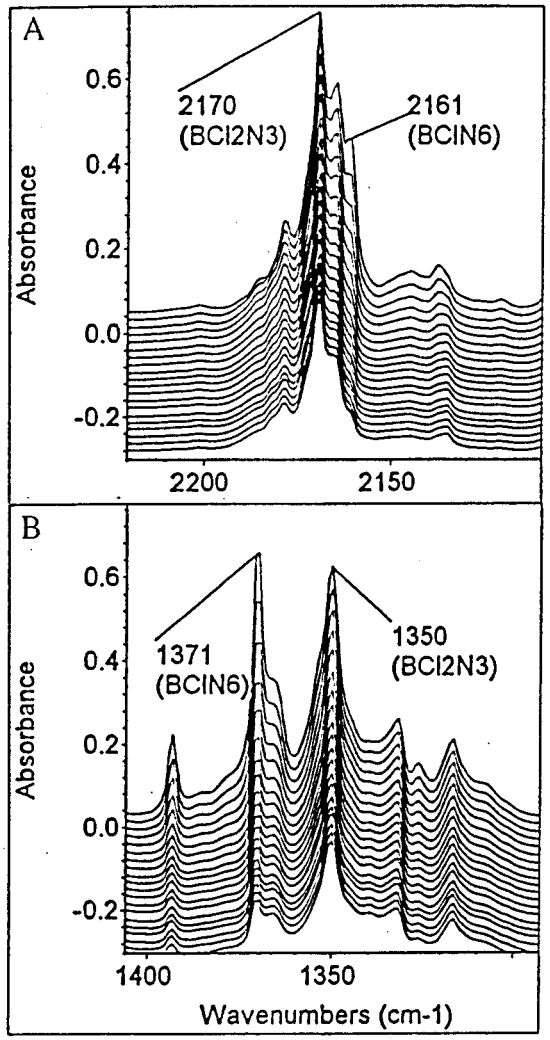

Figure 7. Changes occurring in the IR spectrum during photolysis of an argon matrix containing $BCl_2(N_3)$ and $BCl(N_3)_2$. (A) N_3 asymmetric and (B) BN stretching regions. The top spectrum was taken just before the photolysis began and the bottom spectrum was taken after 1.5 h of photolysis.

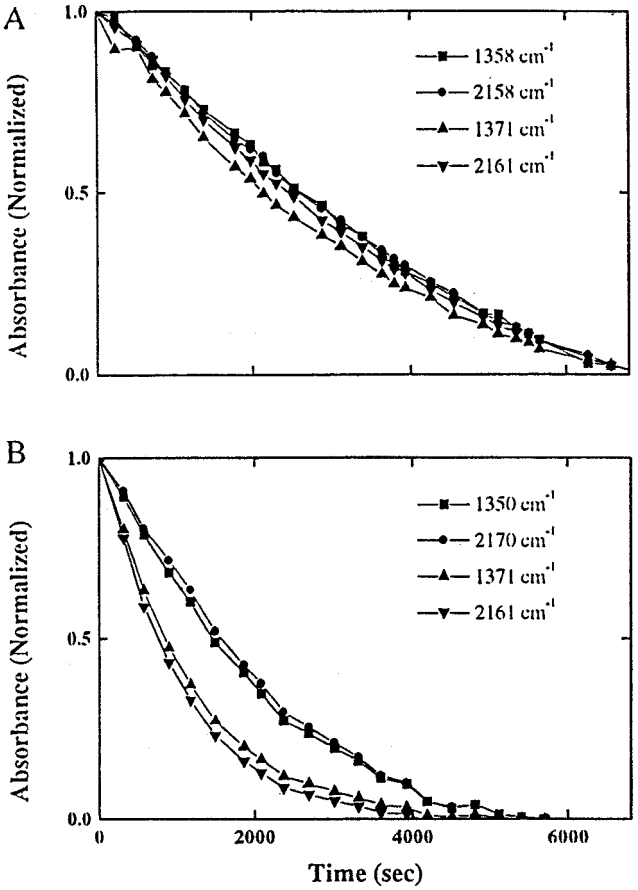

Figure 8. Peak heights plotted vs photolysis time for the parent compounds: (A) from Figure 7, the $B(N_3)_3$ peaks at 1358 and 2158 cm^{-1} and the $BCl(N_3)_2$ peaks at 1371 and 2161 cm^{-1} decay with the same rate; (B) from Figure 8, the BCl_2N_3 peaks at 1350 and 2170 cm^{-1} decay at a faster rate than do the $BCl(N_3)_2$ peaks at 1371 and 2161 cm^{-1}.

TABLE 4: Observed Infrared Maxima for $B(N_3)_3$, $BCl(N_3)_2$, and $BCl_2(N_3)$

	$B(N_3)_3$ (cm^{-1})	$BCl(N_3)_2$ (cm^{-1})	BCl_2N_3 (cm^{-1})
N_3 asymmetric stretch	2158	2161	2170
BN stretch			
^{11}B isotopomer	1358	1371	1350
^{10}B isotopomer	1371	1393	1367
N_3 symmetric stretch			
11B isotopomer	1103		1053
^{10}B isotopomer			1076
BCl stretch			
^{11}B isotopomer		1029	968
^{10}B isotopomer		1060	1010

an initially formed trigonal $BClN_2$ could rearrange to generate three different chain structures: (1) ClNBN formed via Cl atom migration, (2) NBClN formed via N atom migration to the Cl atom, and (3) NNBCl formed via N atom migration to the other N. RCISD/6-311G(D) calculations of these chain compounds did not yield stable, bound structures. Rather, a ring compound, shown in Figure 10 was found to be stable computationally, again using RCISD/6-311G(D). The optimized bond lengths and angles for this molecule are listed in Table 5, and the calculated ground-state frequencies for the ^{10}B and ^{11}B isotopomers are included in Table 6. The calculated frequency of the highest energy vibrational mode is within 2.5% of the observed peak at 1677 cm^{-1}, and the calculated boron isotope shift of 42 cm^{-1} is in very good agreement with the observed shift of 47 cm^{-1}. Visualization[9] of this mode shows it to be a "ring breathing" motion for which there would be very little dipole moment change during the vibration. This correlates well with the fact that the observed feature is very weak. Since this mode is predicted to be the most intense, it is not surprising that no other features were observed in the IR spectrum. However, because this assignment is based on only a single IR feature and its isotopic shift, there is some uncertainty in the assignment. If the assignment is correct, however, it implies that during the rearrangement of the trigonal $BClN_2$, a sufficiently deep well on the potential surface is encountered at the geometry of the ring compound such that the ring compound can persist. The fact that no analogous structures have been observed for BN_3 or BCl_2N reflects the lack of a similar stable point on the potential surfaces for these species. This variation is interesting, and the potential energy surfaces for the three intermediates are under investigation.

Although the product peak at 2050 cm^{-1} remains elusive, it is clear that the species responsible for this feature is photolytically unstable. This feature could be due to the formation of N_2 in close proximity or weakly bound to some other product such that a weak dipole moment is induced in the N_2. The sources of N_2 in this system are the photolysis of $BCl(N_3)_2$ to generate $BClN_2$ and N_2 and a further reaction of the trigonal

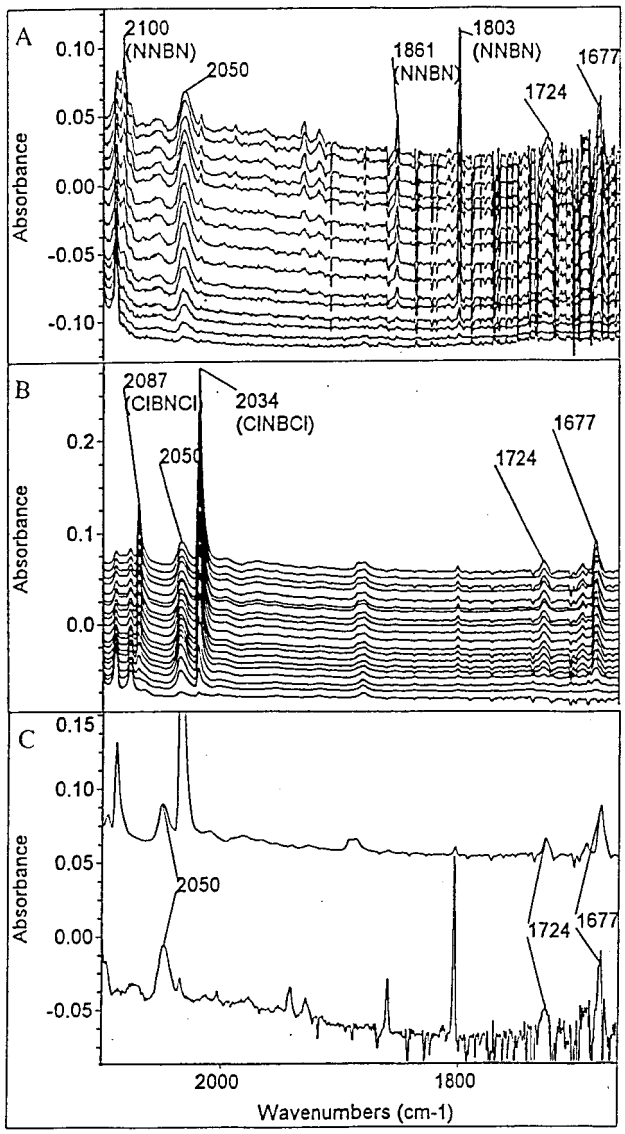

Figure 9. Changes observed between 1650 and 2150 cm^{-1} in the IR spectrum during photolysis of an argon matrix (A) containing $B(N_3)_3$ and $BCl(N_3)_2$ and (B) containing $BCl_2(N_3)$ and $BCl(N_3)_2$. (C) Comparison of the final spectra from (A) and (B). The same peaks are seen to grow in during the photolysis. These data are from the same spectra represented in Figures 7 and 8.

TABLE 5: Optimized Ground State Geometry for $ClBN_2$ (Ring)

parameter	RCISD/6-311G(d) (bond lengths in Å, angles in deg)
B−N	1.4017
N−N	1.2894
B−Cl	1.7063
N−B−N angle	54.7681
B−N−N angle	62.6159
N−B−Cl angle	152.6159

planar intermediate $BClN_2$ generating BCl and N_2. It seems unlikely that the N_2 generated in the first photolysis step of the parent is the source since this feature is not observed following photolysis of matrices that contain only $B(N_3)_3$ or BCl_2N_3 where three and one molecule of N_2 would be generated, respectively. On the other hand, if the source is the $BClN_2$ intermediate, this would suggest that a second rearrangement path for the trigonal intermediate exists leading to NNBCl. This species is not calculated to be bound and is more reasonably represented as two diatomics, N_2 and BCl. The N_2 and BCl would, of course, be located in the same matrix cage, and hence, the BCl could induce the necessary dipole in the N_2, giving rise to the feature at 2050 cm^{-1}. As the photolysis proceeds, local heating could bring about motion in the matrix, causing the N_2 and the BCl to move away from each other and result in a decrease of the 2050 cm^{-1} signal. The vibrational frequency of gaseous BCl is reported to be 839 cm^{-1},[10] and an extremely weak feature at 834 cm^{-1} grows in during photolysis of the 2:1 sample matrix. This may be evidence of BCl formation.

Figure 10. Calculated structure of the ring compound $ClBN_2$.

TABLE 6: Calculated and Observed Infrared Frequencies for $ClBN_2$ (Ring)[a]

	υ_{ring} cm^{-1}
Argon Matrix	
$^{11}ClBN_2$	1677
$^{10}ClBN_2$	1724
difference	47
Calculated Frequencies RCISD/6-311(d)	
$^{11}ClBN_2$	1719
$^{10}ClBN_2$	1762
difference	43

[a] The υ_{ring} mode, an in-plane breathing mode of the three-membered ring, is the most intense mode (calculated intensity = 236 km/mol), and the only detectable feature in the spectrum.

Conclusion

This paper is the third in a series reporting on the results of low-temperature matrix isolation and photolysis studies of the three compounds generated in the room-temperature $BCl_3 + n$ HN_3 gas-phase reaction system, $B(N_3)$, $BCl(N_3)_2$, and BCl_2N_3. In the previous work, $B(N_3)_3$ and BCl_2N_3 were isolated and photolyzed in low-temperature argon matrices, and the photolysis products NNBN and ClBNCl were identified.[3,4] In the work reported here, the results of similar experiments on $BCl(N_3)_2$ are reported.

The photolysis mechanism in all three of these compounds can be described as a two-step process. In the first step, the N−NN bonds of the azide groups are cleaved, a photoprocess that is common to covalent azides,[11−13] leaving a planar trigonal species which, in the second step, rearranges. For the 3:1 and 1:1 compounds, $B(N_3)_3$ and BCl_2N_3, the rearrangement generates NNBN and ClBNCl, respectively, linear compounds that are isoelectronic to the carbon compounds isocyanogen and dichloroacetylene. In the 2:1 compound, $BCl(N_3)_2$, the rearrangement stops when a stable three-membered ring geometry is achieved, and no analogous stable linear structure is generated. A second, photolytically unstable molecule forms as well that has not been identified.

In all of these boron azide matrix studies, the matrix ratios were maintained between 100:1 and 300:1 (Ar/boron azide), and at these ratios there would be aggregate formation in the matrix. No doubt, some of the congestion in the IR spectra can

be attributed to aggregates, but even so, the IR data provide clear differentiation between the three boron azide compounds, $B(N_3)_3$, $BCl(N_3)_2$, and BCl_2N_3. The probable presence of aggregated species has apparently no effect on the photolysis processes in the three compounds. In each case, the isolated photoproduct can be understood in terms of single-molecule photolysis plus rearrangement mechanisms. In addition, the similarity of the mechanisms for the three compounds supports the idea that these are not dependent upon aggregates in the matrix.

Work on these systems is ongoing in our lab. Computational studies of the rearrangement are underway to obtain insight into the similarities and apparent differences of the rearrangement mechanisms. UV/vis absorption studies of the photolysis products are near completion, and LIF studies of the photoproducts are planned.

Acknowledgment. This work was supported by the National Science Foundation under grant CHE-9527080.

References and Notes

(1) Mulinax, R. L.; Okin, G. S.; Coombe, R. D. *J. Phys. Chem.* **1995**, *99*, 6294.

(2) Linnen, C. J.; Macks, D. E.; Coombe, R. D. *J. Phys. Chem.* **1997**, *101*, 1602.

(3) Al-Jihad, I. A.; Liu, B.; Linnen, C. J.; Gilbert, J. V. *J. Phys. Chem.* **1998**, *102*, 6220.

(4) Johnson, L. A.; Sturgis, S. A.; Al-Jihad, I. A.; Liu, B.; Gilbert, J. V. *J. Phys. Chem.* **1999**, *103*, 686.

(5) Andrews, L.; Hassanzadeh, P.; Burkholder, T. R.; Martin, J. M. L. *J. Chem. Phys.* **1993**, *98*, 922.

(6) Hobbs, K.; Coombe, R. D., work in progress.

(7) Schlie, L. A.; Wright, M. W. *J. Chem. Phys.* **1990**, *92*, 394.

(8) *Gaussian 94 (Revision A.1).* Frisch, M. J.; Trucks, G. W.; Schlegel, H. B.; Gill, M. W.; Johnson, B. G.; Robb, M. A.; Cheeseman, J. R.; Keith, T. A.; Petersson, G. A.; Montgomery, J. A.; Raghavachari, K.; Al-Laham, M. A.; Zakrzewski, V. G.; Ortiz, J. V.; Foresman, J. B.; Cioslowski, J.; Stefanov, B. B.; Nanayakkara, A.; Challacombe, M.; Peng, C. Y.; Ayala, P. Y.; Chen, W.; Wong, M. W.; Andres, J. L.; Replogle, E. S.; Gomperts, R.; Martin, R. L.; Fox, D. J.; Binkley, J. S.; Defrees, D. J.; Baker, J.; Stewart, J. P.; Head-Gordon, M.; Gonzalez, C.; Pople, J. A. Gaussian, Inc.: Pittsburgh, PA, 1995.

(9) *AniMol* Version 3.2; Innovative Software, Inc., copyright 1995−96.

(10) Herzberg, G. Molecular Spectra and Molecular Structure; *Spectra of Diatomic Molecules*; Van Nostrand: Princeton, NJ, 1959; Vol. I.

(11) Patel, D; Pritt, A. T., Jr.; Benard, D. J. *J. Phys. Chem.* **1986**, *90*, 1931.

(12) MacDonald, M. A.; David, S. J.; Coombe, R. D. *J. Chem. Phys.* **1986**, *84*, 5513.

(13) Coombe, R. D.; Patel, D.; Pritt, A. T., Jr.; Wodarczk, F. J. *J. Chem. Phys.* **1981**, *75*, 2177.